New Second-order NLO Materials Based on Polymeric Borate Clusters and GeO_4 Tetrahedra: A Combined Experimental and Theoretical Study

Jian-Han Zhang,[a,b] Chun-Li Hu,[a] Fang Kong,[a] Xiang Xu,[a] and Jiang-Gao Mao*[,a]

Supporting Information

Figure S7. The averaged imaginary parts and real parts of dielectric functions for $RbGeB_3O_7$ (a), $Rb_2GeB_4O_9$ (b) and $Rb_4Ge_3B_6O_{17}$ (c).

Figure S8. The dispersion of refractive index for $RbGeB_3O_7$ (a), $Rb_2GeB_4O_9$ (b) and $Rb_4Ge_3B_6O_{17}$ (c).

Figure S9. Frequency-dependent SHG coefficients for $RbGeB_3O_7$ (a), $Rb_2GeB_4O_9$ (b) and $Rb_4Ge_3B_6O_{17}$ (c).

Table S1. The state energies (eV) of the lowest conduction band (L-CB) and the highest valence band (H-VB) of the crystal $RbGeB_3O_7$, $Rb_2GeB_4O_9$ and $Rb_4Ge_3B_6O_{17}$.

Compound	k-point	L-CB	H-VB
$RbGeB_3O_7$	G (0.000, 0.000, 0.000)	4.18781	0
	Z (0.000, 0.000, 0.500)	5.01397	-0.11492
	T (-0.500, 0.000, 0.500)	5.53395	-0.1781
	Y (-0.500, 0.000, 0.000)	4.92027	-0.08679
	S (-0.500, 0.500, 0.000)	5.28936	-0.11626
	X (0.000, 0.500, 0.000)	4.79644	-0.09125
	U (0.000, 0.500, 0.500)	5.12676	-0.10755
	R (-0.500, 0.500, 0.500)	5.56488	-0.106
$Rb_2GeB_4O_9$	Z (0.000, 0.000, 0.500)	3.83946	-0.01677
	G (0.000, 0.000, 0.000)	3.54292	-0.01575
	Y (0.000, 0.500, 0.000)	4.10641	-0.0156

	A (-0.500, 0.500, 0.000)	4.70984	-0.03025
	B (-0.500, 0.000, 0.000)	4.6333	0
	D (-0.500, 0.000, 0.500)	4.67948	-0.00392
	E (-0.500, 0.500, 0.500)	4.72426	-0.03185
	C (0.000, 0.500, 0.500)	4.23716	-0.01901
$Rb_4Ge_3B_6O_{17}$	Z (0.000, 0.000, 0.500)	3.4668	-0.01247
	G (0.000, 0.000, 0.000)	3.28767	-0.00562
	Y (0.000, 0.500, 0.000)	4.08426	-0.01712
	A (-0.500, 0.500, 0.000)	4.15936	0
	B (-0.500, 0.000, 0.000)	3.7399	-0.00881
	D (-0.500, 0.000, 0.500)	3.73418	-0.01396
	E (-0.500, 0.500, 0.500)	4.14883	-3.21366E-4
	C (0.000, 0.500, 0.500)	4.14532	-0.02614

Table S2. The calculated bond orders of $RbGeB_3O_7$, $Rb_2GeB_4O_9$ and $Rb_4Ge_3B_6O_{17}$.

For $RbGeB_3O_7$					
Bond	Bond length	Bond order	Bond	Bond length	Bond order
B-O	1.33147	0.91	B-O	1.33985	0.90
B-O	1.36752	0.82	B-O	1.36945	0.80
B-O	1.38522	0.77	B-O	1.39849	0.76
B-O	1.45076	0.68	B-O	1.47611	0.65
B-O	1.48696	0.61	B-O	1.48857	0.62
Ge-O	1.72126	0.54	Ge-O	1.73072	0.62
Ge-O	1.74479	0.52	Ge-O	1.75789	0.49

For $Rb_2GeB_4O_9$					
Bond	Bond length	Bond order	Bond	Bond length	Bond order
B-O	1.33645	0.88	B-O	1.34219	0.87
B-O	1.34588	0.81	B-O	1.34871	0.88
B-O	1.36014	0.88	B-O	1.36236	0.87
B-O	1.36755	0.88	B-O	1.37751	0.86
B-O	1.37771	0.86	B-O	1.38182	0.77
B-O	1.38342	0.76	B-O	1.40440	0.76
B-O	1.41021	0.75	B-O	1.42459	0.69
B-O	1.43964	0.72	B-O	1.44236	0.69
B-O	1.44654	0.68	B-O	1.44984	0.72
B-O	1.46265	0.70	B-O	1.47930	0.63
B-O	1.48228	0.60	B-O	1.49627	0.60
B-O	1.49849	0.61	B-O	1.49852	0.59
B-O	1.49867	0.59	B-O	1.50030	0.59
B-O	1.51266	0.59	B-O	1.51524	0.57
Ge-O	1.72654	0.58	Ge-O	1.72993	0.63
Ge-O	1.73517	0.60	Ge-O	1.74242	0.58
Ge-O	1.74589	0.50	Ge-O	1.74681	0.49
Ge-O	1.75590	0.46	Ge-O	1.75773	0.52
For $Rb_4Ge_3B_6O_{17}$					
Bond	Bond length	Bond order	Bond	Bond length	Bond order
B-O	1.34743	0.89	B-O	1.34872	0.89
B-O	1.35847	0.87	B-O	1.37050	0.79
B-O	1.38827	0.88	B-O	1.39079	0.76
B-O	1.40048	0.76	B-O	1.40666	0.71
B-O	1.41616	0.68	B-O	1.41918	0.75
B-O	1.43432	0.66	B-O	1.45146	0.73
B-O	1.46027	0.65	B-O	1.48528	0.63

B-O	1.50870	0.58	B-O	1.50893	0.58
B-O	1.51121	0.59	B-O	1.51801	0.69
B-O	1.51806	0.59	B-O	1.55402	0.60
B-O	1.55596	0.58	B-O	1.56021	0.59
Ge-O	1.67042	0.63	Ge-O	1.67769	0.51
Ge-O	1.68741	0.54	Ge-O	1.69709	0.56
Ge-O	1.70497	0.67	Ge-O	1.71665	0.58
Ge-O	1.72862	0.64	Ge-O	1.73014	0.62
Ge-O	1.77111	0.52	Ge-O	1.84528	0.49
Ge-O	1.84621	0.55	Ge-O	1.85544	0.57

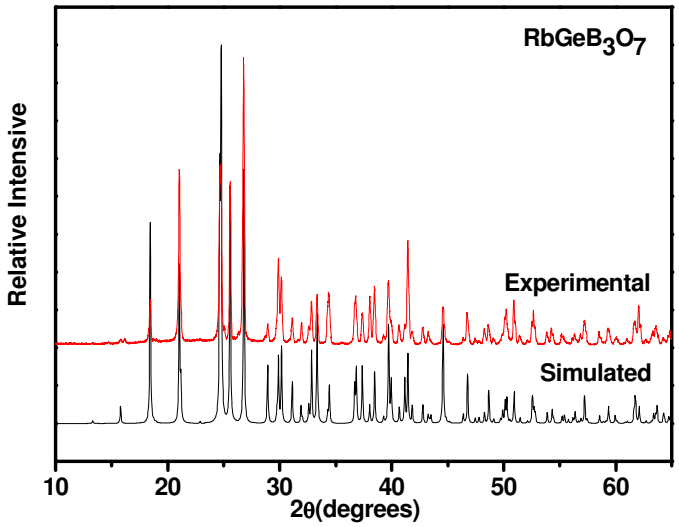

(b)

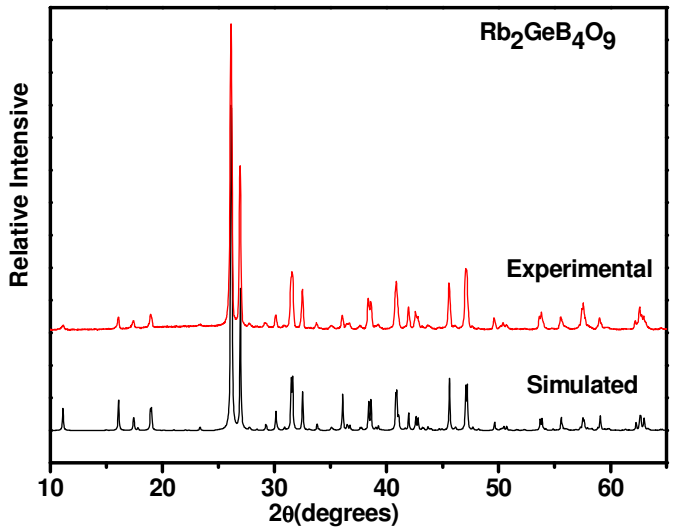

(a)

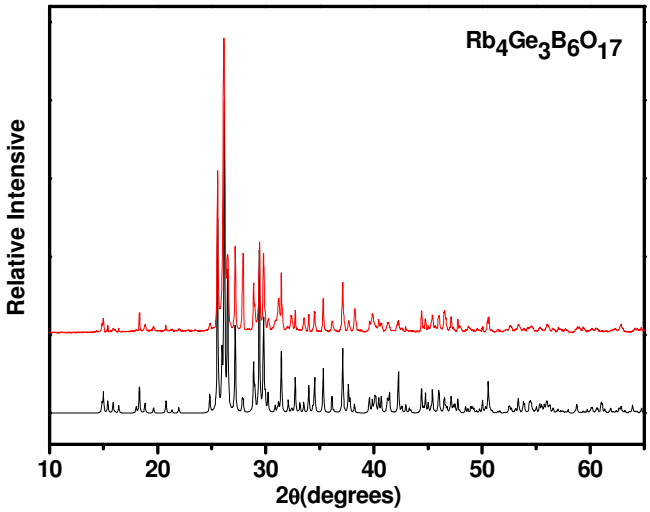

(c)

Figure S1. Simulated and measured XRD powder patterns for $RbGeB_3O_7$ (a), $Rb_2GeB_4O_9$ (b) and $Rb_4Ge_3B_6O_{17}$ (c).

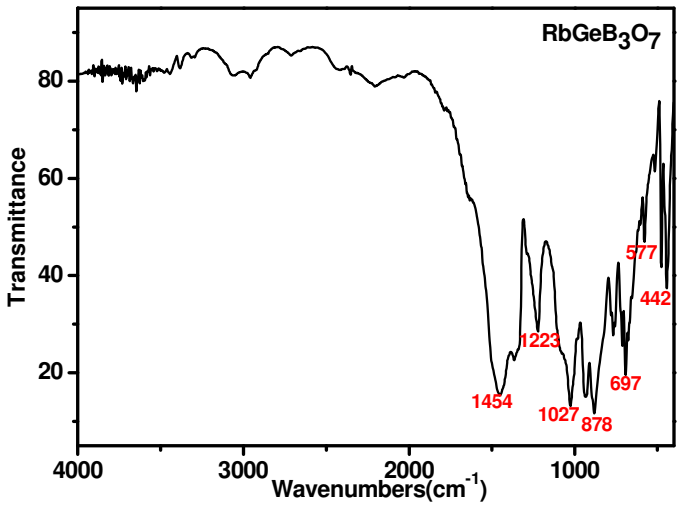

(a)

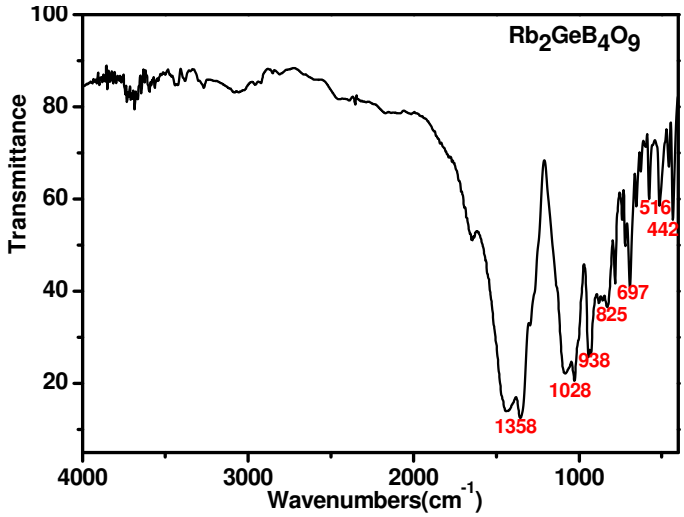

(b)

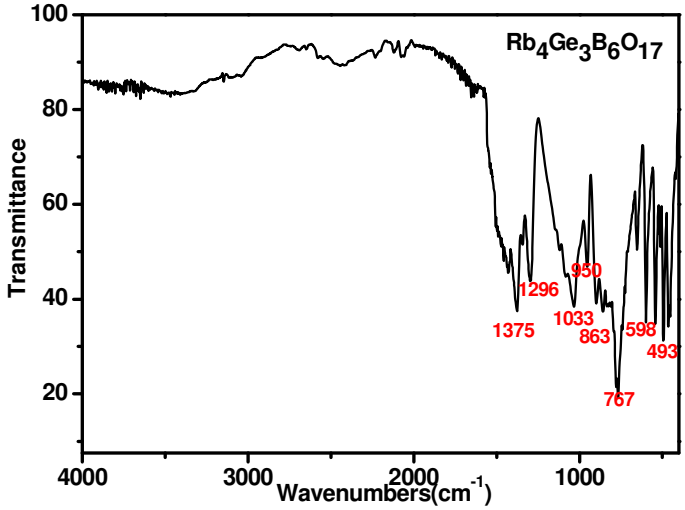

(c)

Figure S2. IR spectra for $RbGeB_3O_7$ (a), $Rb_2GeB_4O_9$ (b) and $Rb_4Ge_3B_6O_{17}$ (c).

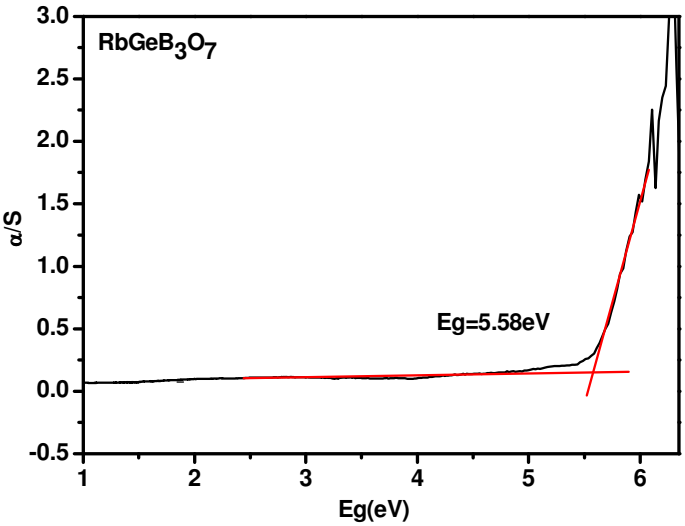

(a)

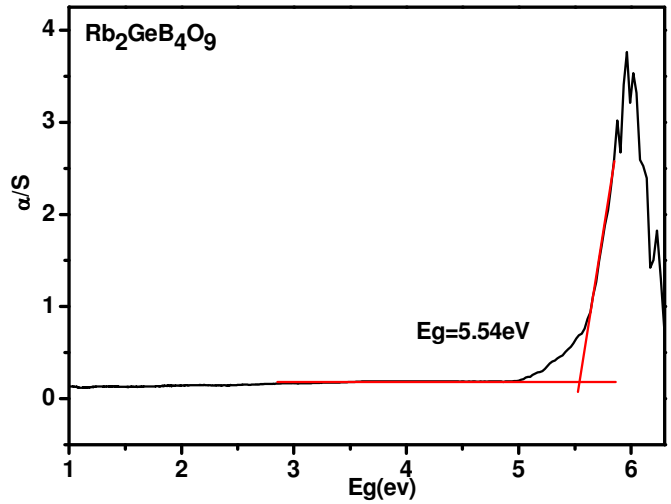

(b)

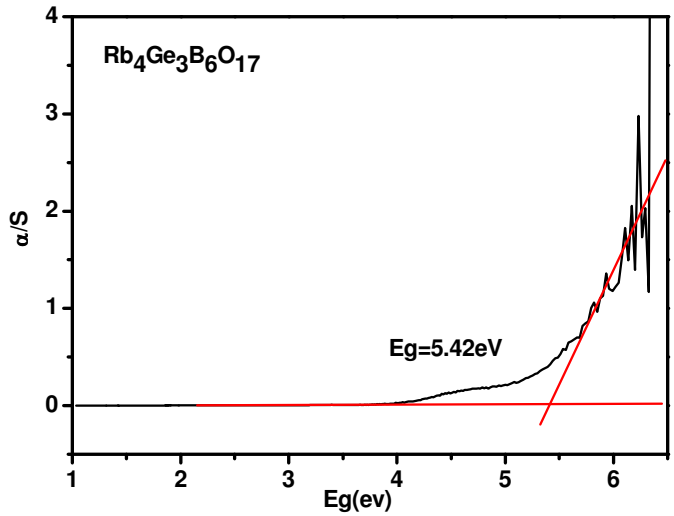

(c)

Figure S3. Optical diffuse reflectance spectra for $RbGeB_3O_7$ (a), $Rb_2GeB_4O_9$ (b) and $Rb_4Ge_3B_6O_{17}$ (c).

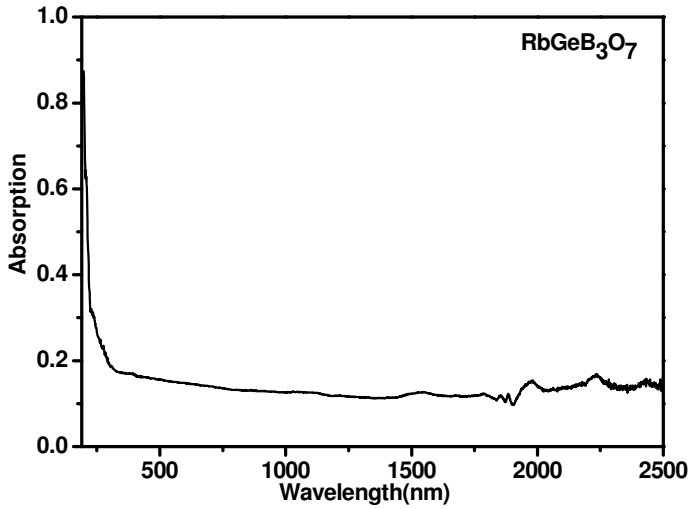

(a)

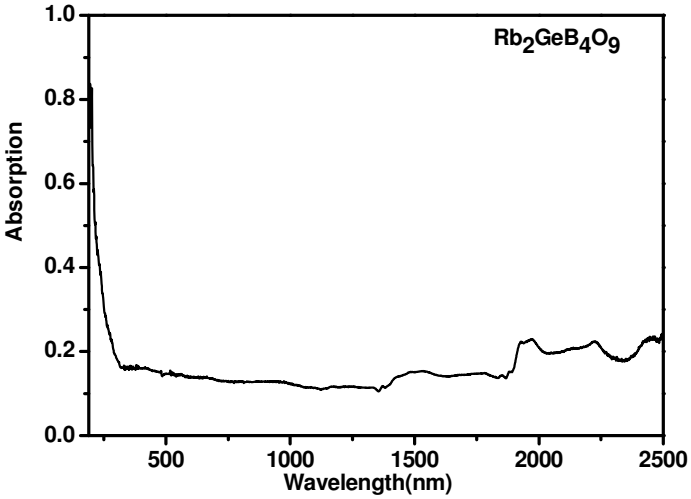

(b)

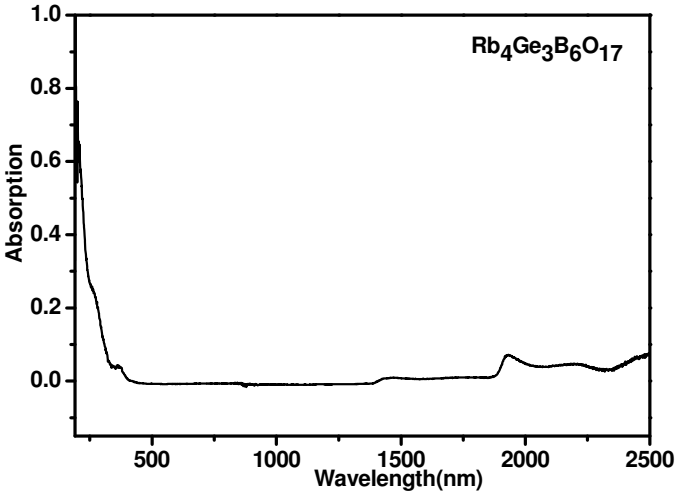

(c)

Figure S4. UV absorption spectra of $RbGeB_3O_7$ (a), $Rb_2GeB_4O_9$ (b) and $Rb_4Ge_3B_6O_{17}$ (c).

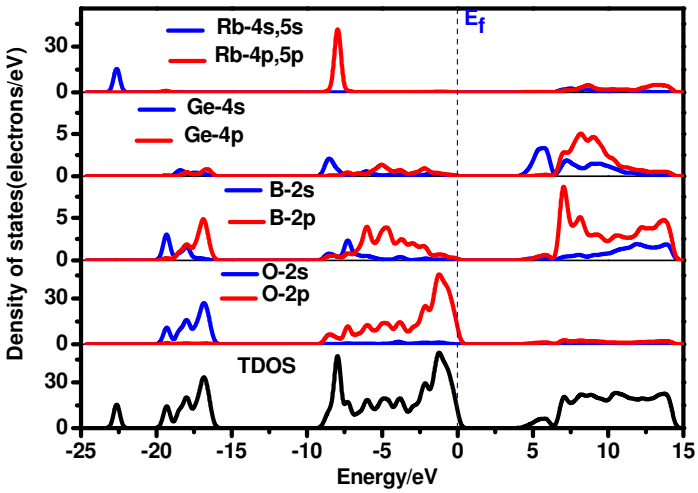

(a)

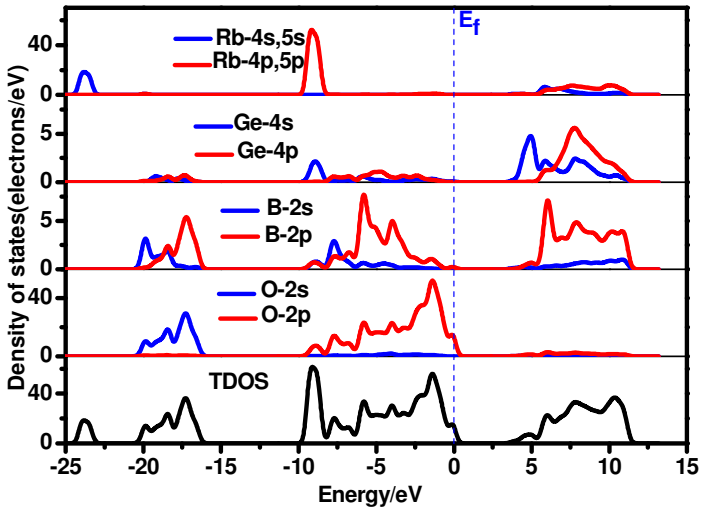

(b)

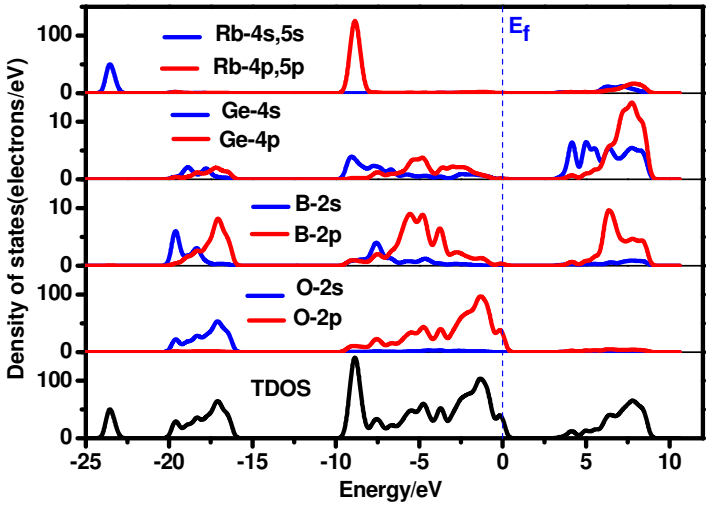

(c)

Figure S5. Total density of states and partial density of states of $RbGeB_3O_7$ (a), $Rb_2GeB_4O_9$ (b) and $Rb_4Ge_3B_6O_{17}$ (c). The Fermi level is set at 0 eV.

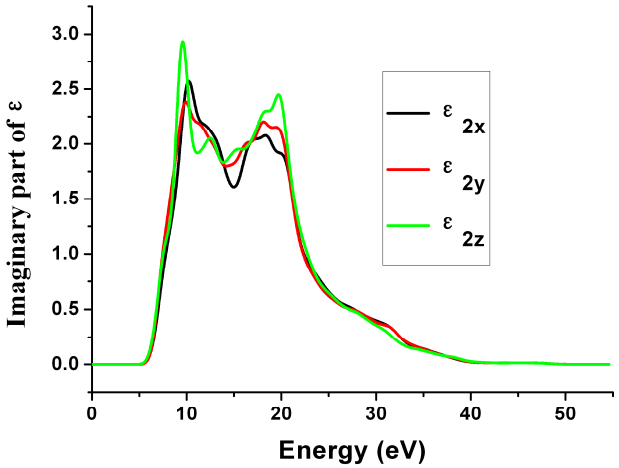

(a)

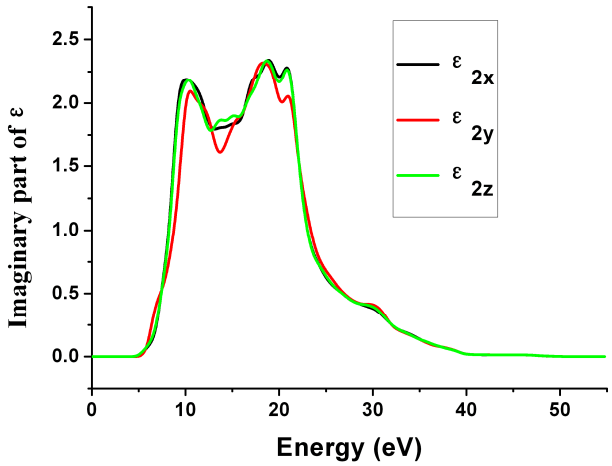

(b)

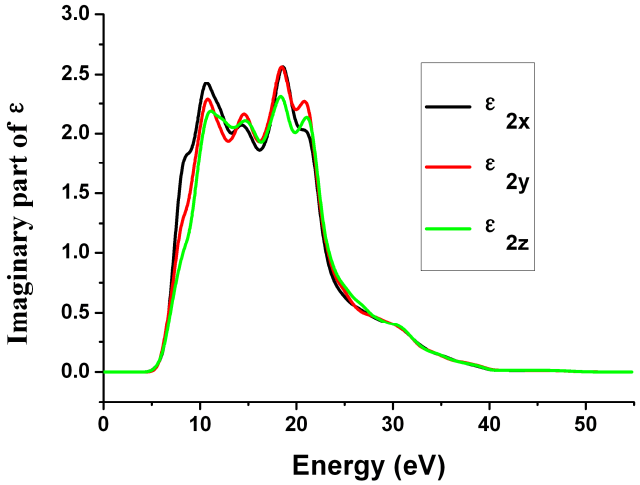

(c)

Figure S6. The imaginary parts of the frequency-dependent dielectric functions of $RbGeB_3O_7$ (a), $Rb_2GeB_4O_9$ (b) and $Rb_4Ge_3B_6O_{17}$ (c).

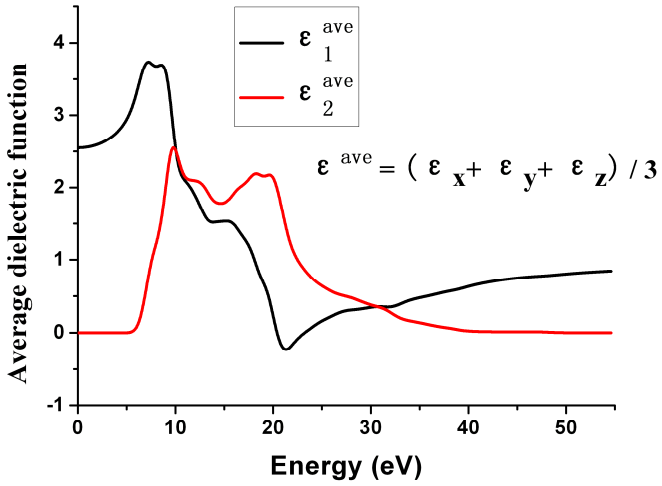

(a)

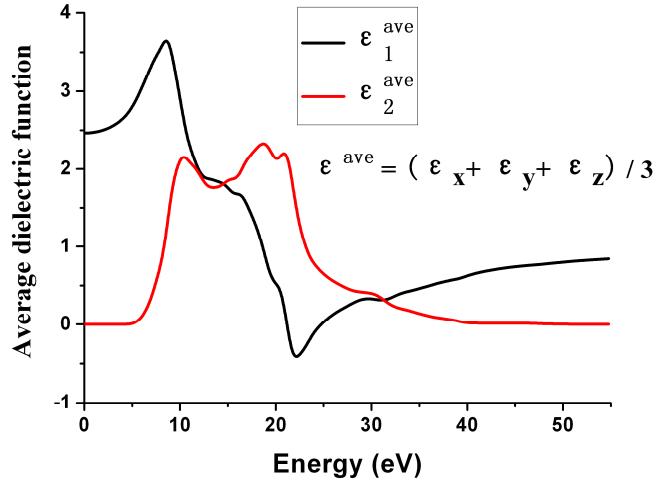

(b)

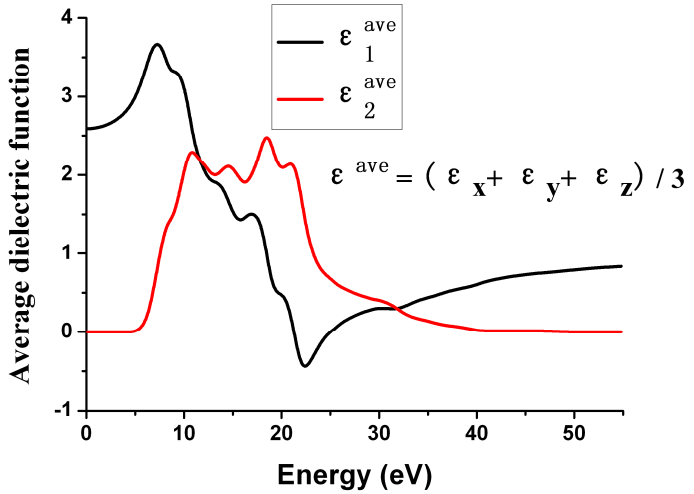

(c)

Figure S7. The averaged imaginary parts and real parts of dielectric functions for $RbGeB_3O_7$ (a), $Rb_2GeB_4O_9$ (b) and $Rb_4Ge_3B_6O_{17}$ (c).

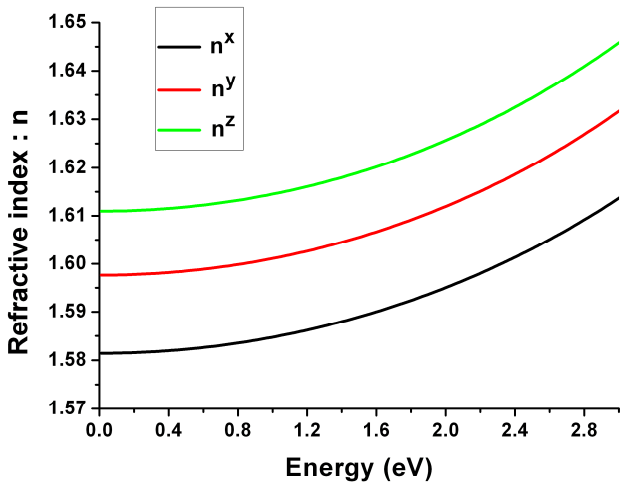

(a)

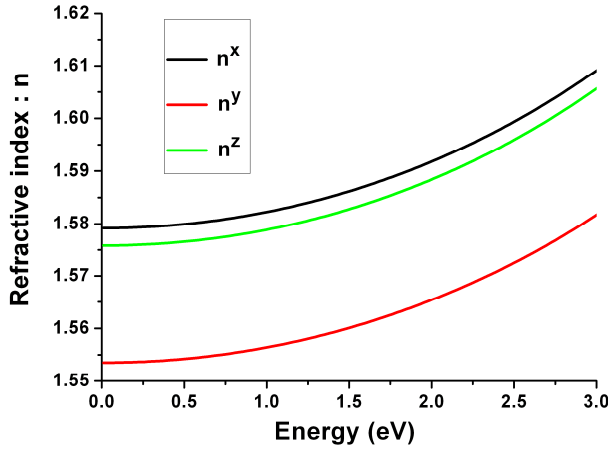

(b)

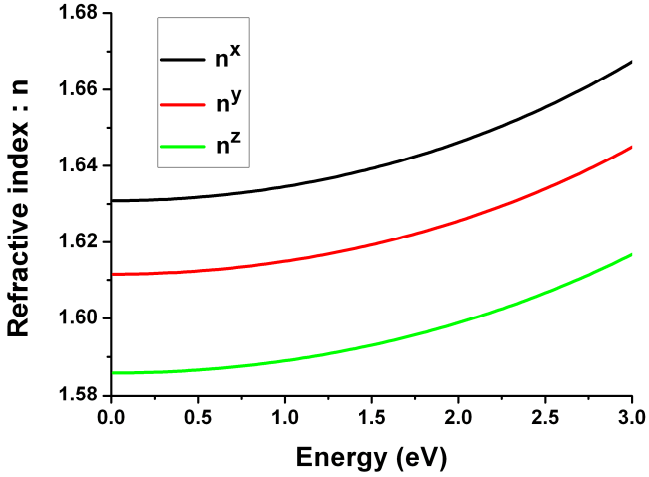

(c)

Figure S8. The dispersion of refractive index for $RbGeB_3O_7$ (a), $Rb_2GeB_4O_9$ (b) and $Rb_4Ge_3B_6O_{17}$ (c).

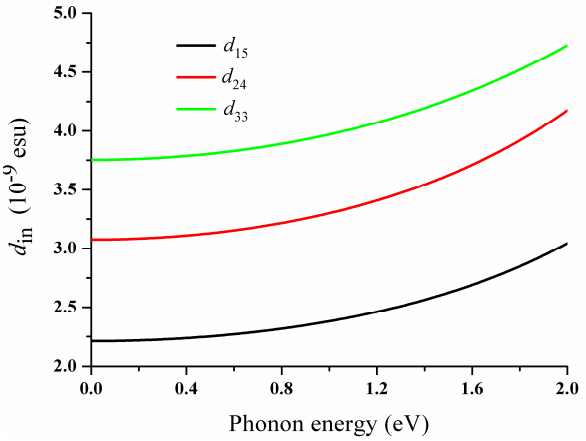

(a)

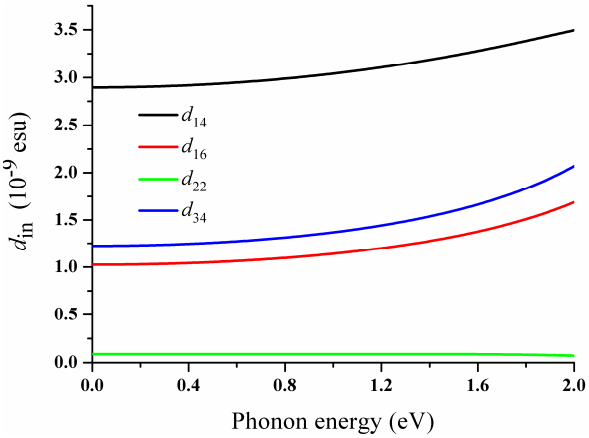

(b)

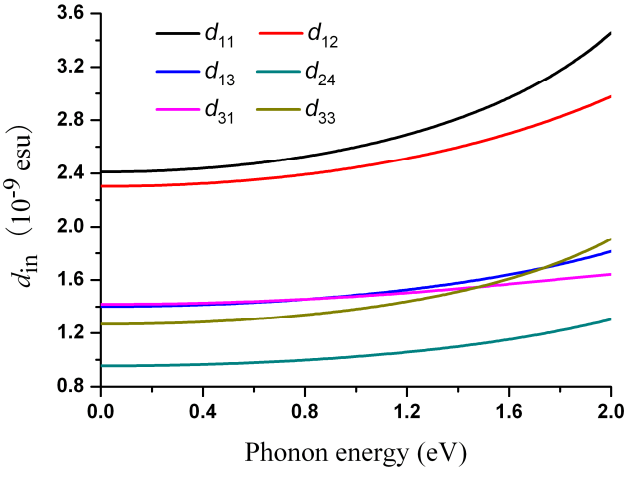

(c)

Figure S9. Frequency-dependent SHG coefficients for $RbGeB_3O_7$ (a), $Rb_2GeB_4O_9$ (b) and $Rb_4Ge_3B_6O_{17}$ (c).